Changes in membrane properties of rat deep cerebellar nuclear projection neurons during acquisition of eyeblink conditioning

Desheng Wang[a,b,c,1], Carrie A. Smith-Bell[a,b,c], Lauren B. Burhans[a,b,c], Deidre E. O'Dell[a,b,c], Roger W. Bell[a,b,c], and Bernard G. Schreurs[a,b,c,1]

[a]Department of Physiology and Pharmacology, West Virginia University School of Medicine, Morgantown, WV 26506; [b]Department of Neuroscience, West Virginia University School of Medicine, Morgantown, WV 26506; and [c]Rockefeller Neuroscience Institute, West Virginia University School of Medicine, Morgantown, WV 26506

Previous studies have shown changes in membrane properties of neurons in rat deep cerebellar nuclei (DCN) as a function of development, but due to technical difficulties in obtaining viable DCN slices from adult animals, it remains unclear whether there are learning-related alterations in the membrane properties of DCN neurons in adult rats. This study was designed to record from identified DCN cells in cerebellar slices from postnatal day 25–26 (P25–26) rats that had a relatively mature sensory nervous system and were able to acquire learning as a result of tone–shock eyeblink conditioning (EBC) and to document resulting changes in electrophysiological properties. After electromyographic electrode implantation at P21 and inoculation with a fluorescent pseudorabies virus (PRV-152) at P22–23, rats received either four sessions of paired delay EBC or unpaired stimulus presentations with a tone conditioned stimulus and a shock unconditioned stimulus or sat in the training chamber without stimulus presentations. Compared with rats given unpaired stimuli or no stimulus presentations, rats given paired EBC showed an increase in conditioned responses across sessions. Whole-cell recordings of both fluorescent and nonfluorescent DCN projection neurons showed that delay EBC induced significant changes in membrane properties of evoked DCN action potentials including a reduced after-hyperpolarization amplitude and shortened latency. Similar findings were obtained in hyperpolarization-induced rebound spikes of DCN neurons. In sum, delay EBC produced significant changes in the membrane properties of juvenile rat DCN projection neurons. These learning-specific changes in DCN excitability have not previously been reported in any species or task.

eyeblink conditioning | deep cerebellar nuclei | intrinsic membrane properties | whole-cell recording | after-hyperpolarization

Eyeblink conditioning (EBC) has been widely regarded as a good model for studying the neural mechanisms underlying learning and memory because of the well-understood neural circuitry and the well-defined parameters influencing the rate and strength of EBC (1–4). The basic cerebellar circuitry underlying tone–shock EBC comprises sensory inputs that reach deep cerebellar nuclei (DCN) and the cerebellar cortex via auditory and trigeminal sensory pathways that give rise to mossy fibers and climbing fibers, respectively (5–7). DCN, a major convergence and integration site for tone–shock associations and also the sole output from the cerebellum, is crucial to the ontogeny of eyeblink conditioned responses because learning-related synaptic plasticity at this essential neuronal substrate has been revealed as a result of stimulation of both excitatory (8–10) and inhibitory (10–13) inputs and thus has been a target for exploring the encoding and decoding of learning and memory.

Rat conditioned eyeblink responses following tone–shock pairings do not emerge reliably until postnatal day 20 (P20) (4) due to significant developmental changes in DCN during the first few postnatal weeks (14–16) and the maturation of sensory processing (17–19). To understand the role of the adult DCN in EBC, experiments have used lesions (20), inactivation (21), stimulation (22), histological examination (23), and in vivo extracellular re-

cordings (24). However, none of these methods has been able to identify changes in individual DCN projection neurons involved in EBC. Moreover, in vitro whole-cell recordings of DCN neurons have heretofore not been reported in adult animals due to the difficulties in obtaining viable DCN slices from adults and technical problems obtaining patch clamp recordings from adult DCN neurons caused by an extensive perineuronal net surrounding more than 93% of neurons in adult mammals (25–27).

The current experiments sought to identify DCN projection neurons involved in the eyeblink response using pseudorabies virus PRV-152 as a fluorescent transsynaptic neuronal tracer (28) and to investigate changes in intrinsic membrane properties that result from the acquisition of EBC by using a new slicing technique (16) to obtain healthy acute DCN slices from P25–26 rats that had passed through the narrow DCN development window at P22–25 (16), had a relatively mature sensory and auditory system, and were able to acquire learning as a result of tone–shock EBC (18, 29, 30). Optimizing the transit time for PRV-152 to reach the DCN, using rats of the oldest age at which patch-clamp recordings could still be obtained, and taking into account the level of EBC shown by rats at that age, we examined slices from rats given four sessions of EBC, which resulted in modest levels of conditioning. As a result, we examined the membrane properties of projection neurons during the acquisition of EBC rather than at its terminal levels. To date, there are no reports of learning-related changes in the membrane properties of individual neurons in the DCN.

Significance

Although large ensembles of neurons have been found to change as a function of learning and memory, localizing those changes to the individual neurons directly involved in a specific task has been challenging. Using whole-cell recording of deep cerebellar nuclear neurons (DCN) and a transsynaptic viral tracer, we found motor learning induced significant changes in membrane properties of rat DCN projection neurons including a reduced after-hyperpolarization amplitude and shortened latency for both evoked DCN action potentials and rebound spikes. These learning-specific changes in DCN excitability have not previously been reported in any species or task.

www.manaraa.com

Results

Delay EBC. Fig. 1*A* depicts the delay conditioning paradigm employed in the experiment and the well-defined underlying neuronal circuit showing that DCN is a convergence site for input signals from both the shock unconditioned stimulus (US) climbing fiber pathway and the tone conditioned stimulus (CS) parallel mossy fiber pathway and the sole output pathway for motor responses. Fig. 1*B* shows the mean percent of conditioned response (CR) levels for rats exposed to paired or unpaired tone–shock presentations and for rats that were exposed to the apparatus but received no stimulus presentations (Paired, Unpaired, and Sit groups, respectively), and the inset shows the magnitude of CRs. Compared with the rats in the Unpaired and Sit groups, rats in the Paired group showed a significantly greater
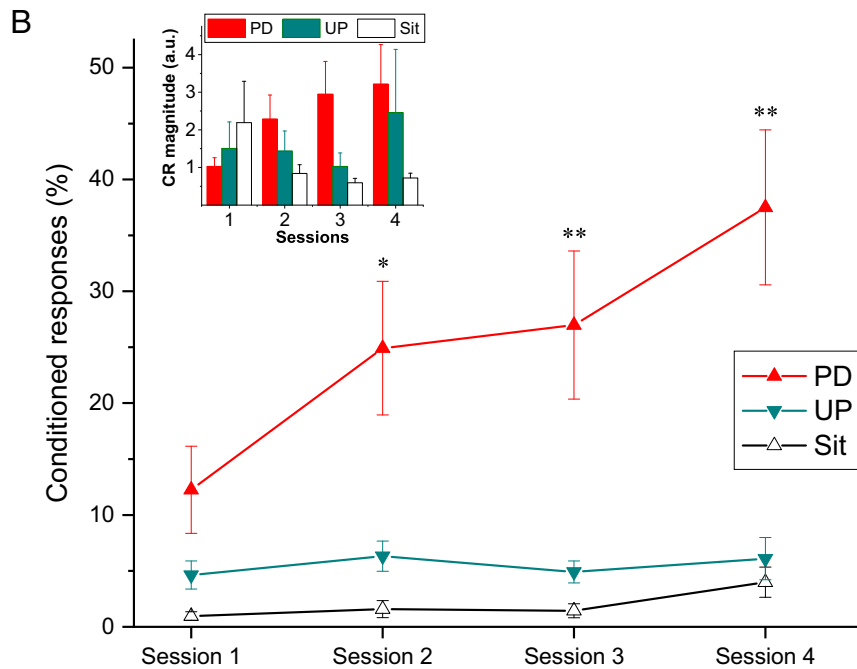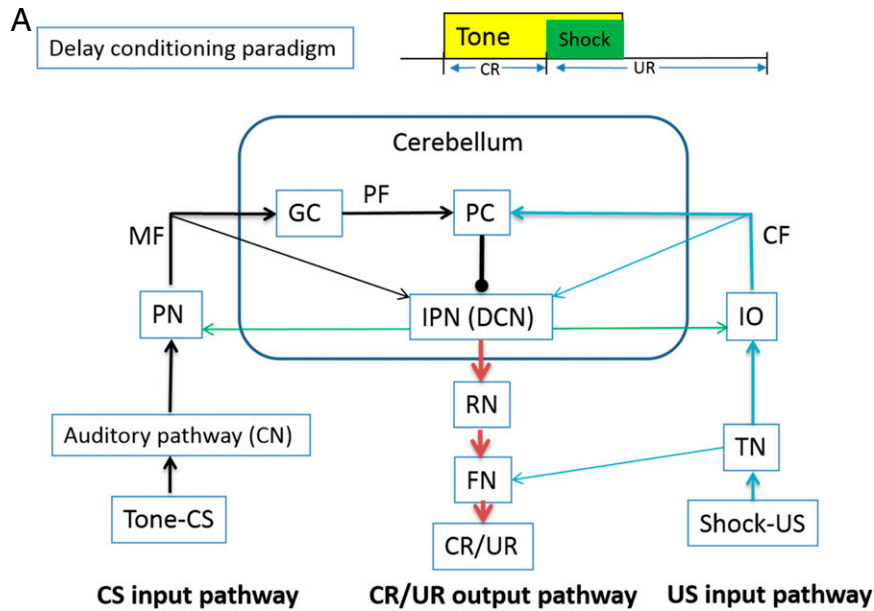

Fig. 1. The mean percent (±SEM) of CRs during delay eyeblink conditioning. (*A*) The delay conditioning paradigm and the underlying neuronal circuitry. (*B*) The mean percent CRs (CRs%) for rats in the Paired (PD), Unpaired (UP), and Sit groups. The *Inset* in *B* shows that the CR magnitude for the Paired group increased with training sessions compared with Unpaired and Sit groups. Note that the Paired group showed greater CRs% than the Unpaired and Sit groups across the four sessions of delay eyeblink conditioning, which suggests the acquisition of learning. Asterisks denote values for the Paired group that are significantly different from those for the Unpaired and Sit groups (*$P < 0.05$, **$P < 0.01$). CF, climbing fiber; CN, cochlear nucleus; FN, facial nucleus; GC, granule cell; IO, inferior olive; IPN, interpositus nucleus; MF, mossy fiber; PC, Purkinje cell; PF, parallel fiber; PN, pontine nuclei; RN, red nucleus; TN, trigeminal nucleus; UR, unconditioned response.

www.manaraa.com

percentage of CRs across sessions, reaching a mean level of 40% CRs by the fourth session, indicating the acquisition of delay EBC. This was confirmed by an ANOVA of the percent of CRs that revealed significant main effects of sessions [$F(3, 75) = 5.035$, $P < 0.01$] and group [$F(2, 25) = 6.054$, $P < 0.01$] and an interaction between sessions and group [$F(6, 75) = 5.524$, $P < 0.001$]. Post hoc comparisons revealed that the group effect in percent CRs was attributable to a significant difference between the Paired group and the Unpaired and Sit groups (all $Ps < 0.05$). Statistical analysis of the percent of responses on tone-alone test trials showed a similar group effect [$F(2, 24) = 8.817$, $P < 0.01$]. The CR magnitude for the Paired group increased with training sessions compared with that for both the Unpaired and Sit groups, which was confirmed by a group × sessions interaction [$F(2, 81) = 2.452$, $P < 0.05$]. These data confirm that rats with relatively mature sensory and motor processing were able to acquire a significant level of eyeblink-conditioned responses when trained for only four sessions at P23–24 with tone–shock paired EBC.

Identification of DCN Projection Neurons by PRV-152. To identify DCN projection neurons responsible for the eyeblink response, PRV-152, a transsynaptic neuronal tracer, was injected into the orbicularis oculi muscle. As shown in Fig. 2, anti-PRV immunolabeling showed labeled first-order motor neurons in the dorsolateral facial nucleus ipsilaterally (Fig. 2 A and B), labeled second-order premotor neurons in the contralateral red nucleus (Fig. 2 C and D) at 2.5 d following PRV inoculation, labeled

third-order premotor neurons mainly in ipsilateral DCN (Fig. 2 E and F) at 3 d following PRV inoculation, and extensive labeled neurons in the DCN at 3.5 d following PRV inoculation (Fig. 2 E and G). These data suggest that PRV-152 could be reliably taken up by axon terminals of facial nucleus neurons and retrogradely transported to DCN projection neurons via the contralateral red nucleus, which is similar to previous reports (28, 31, 32).

Membrane Properties. To map the changes in membrane properties of the DCN resulting from the behavioral manipulations, whole-cell current-clamp recordings were performed on 62 DCN neurons, 20 of which were from fluorescent DCN neurons. As shown in Fig. 3 and described in our previous publication (16), neurons in the DCN were spontaneously active at resting membrane potential and showed action potential (AP) firing in response to depolarizing current injections when held at −70 mV. Measurements of spontaneous APs revealed no significant differences among Paired, Unpaired, and Sit groups. As shown in Table 1, there were no statistical differences (all $Ps > 0.05$) in membrane properties between fluorescent and nonfluorescent DCN neurons, so the data collected from these two types of DCN neurons were combined. Fig. 3A, Lower Inset shows a representative biocytin-filled DCN neuron in which a whole-cell recording was made with 0.2% biocytin in the recording electrode and visualized later by the avidin-biotin complex method. The DCN neuron appeared to be largely multipolar with dendrite processes, which is consistent with the large multipolar glutamatergic projection neurons in previous reports (33, 34).
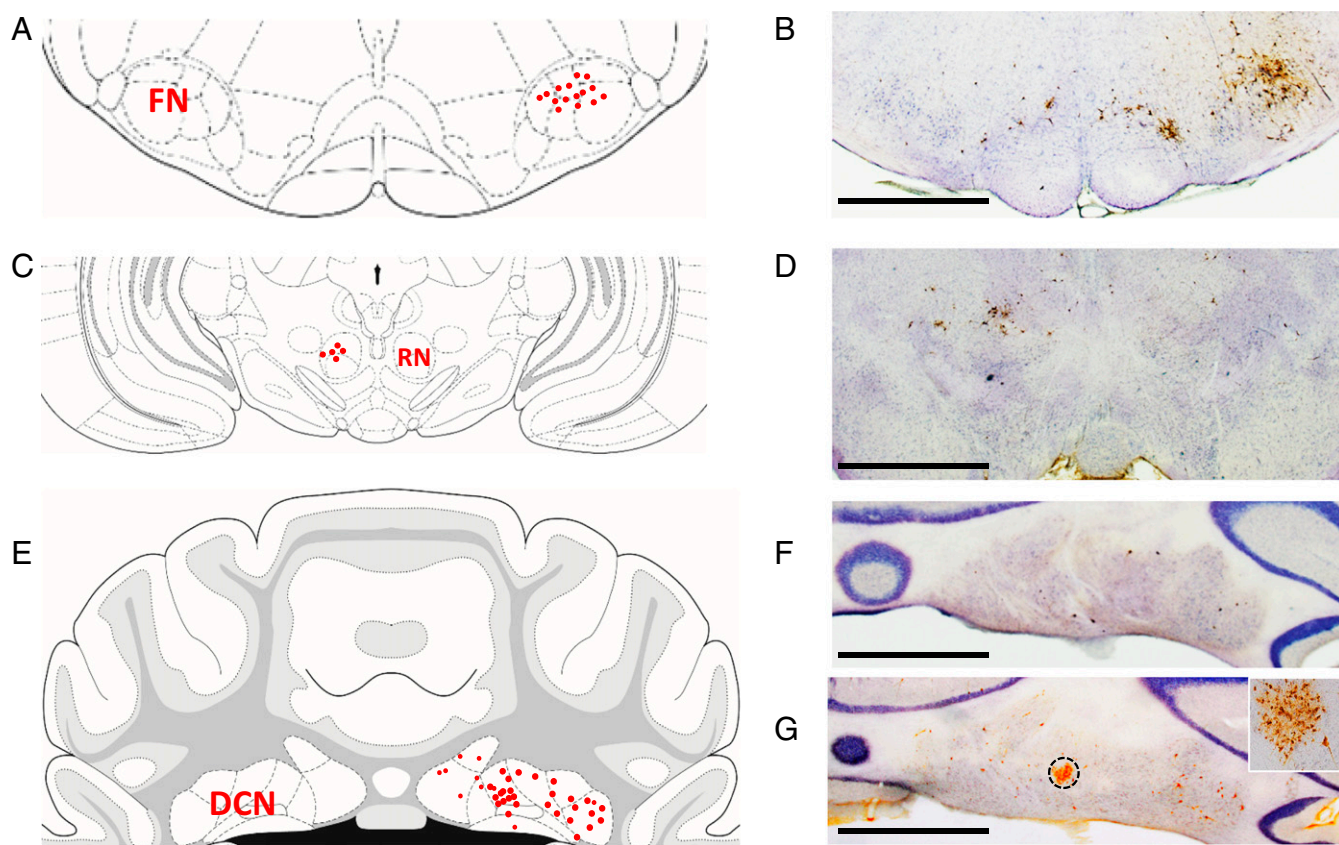

Fig. 2. Identification of DCN projection neurons by the transsynaptic neuronal tracer PRV-152. (A, C, and E) The distribution of PRV-labeled neurons in FN (A), RN (C), and DCN (E). (B, D, F, and G) Representative PRV-labeled neurons in the FN (B), RN (D), and DCN (F and G) which were identified by anti-PRV immunolabeling. Atlas images were modified from ref. 79. All light microscope images were taken with a 1.25× microscope objective. (Scale bars: 500 μm.) The Inset in G was taken with microscope with a 10× objective from the DCN area indicated by dashed circle. Note that PRV-152 was injected into orbicularis oculi muscle of the upper eyelid, taken up by axon terminals of FN neurons, retrogradely transported to the RN, and reached the DCN after 3 d of PRV inoculation. Extensive PRV-infected DCN neurons were observed after 3.5 d of PRV inoculation.
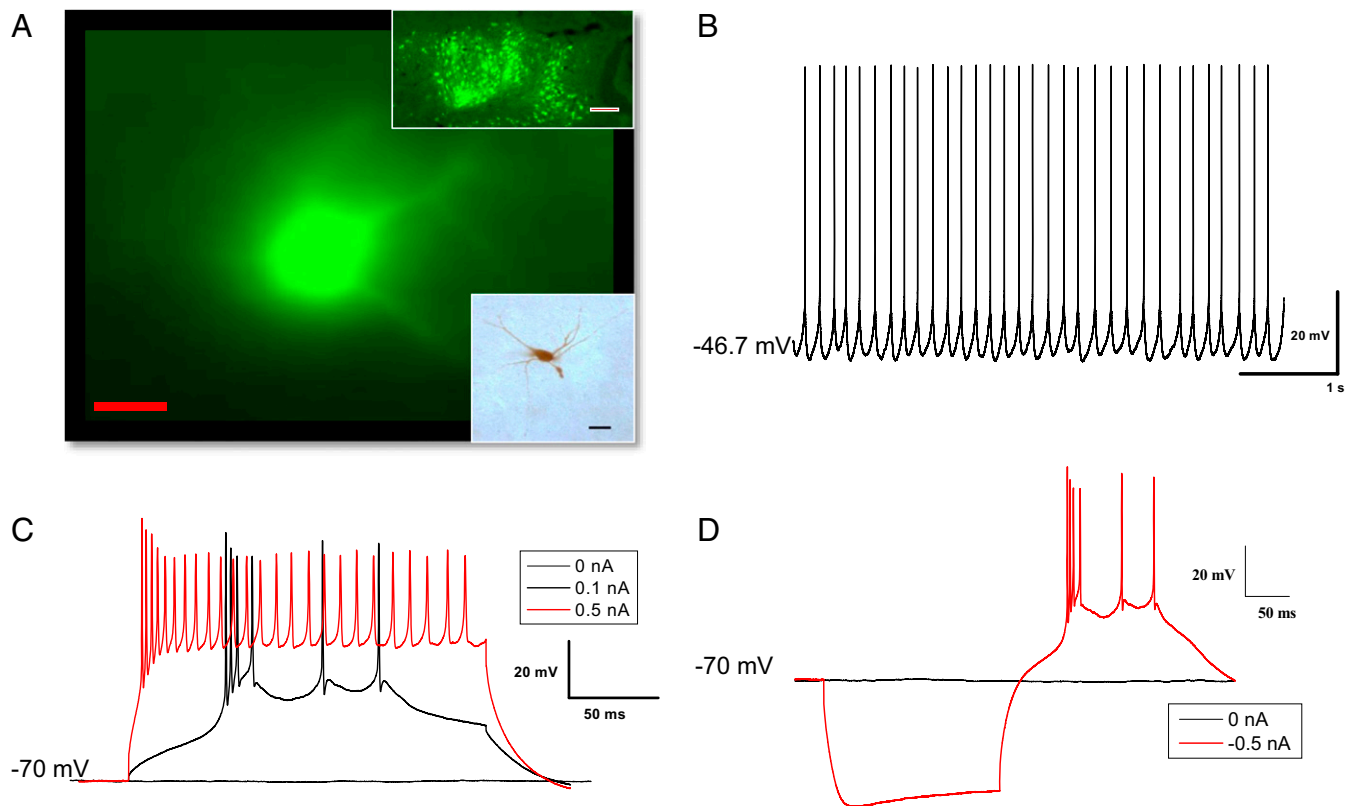
Wang et al.

www.manaraa.com

Fig. 3. Typical recording traces from a representative rat DCN cell. (*A*) A representative fluorescent DCN cell retrogradely tracked from the eyelid with PRV-152. (Scale bar: 20 μm.) (*Upper Inset*) There are extensive fluorescent neurons in DCN area. (Magnification: 4×.) (Scale bar: 200 μm.) (*Lower Inset*) A biocytin-filled DCN neuron that was detected with the avidin-biotin complex method. (Scale bar: 50 μm.) (*B–D*) Typical recordings at a resting membrane potential of −47.6 mV (*B*), responding to 200-ms depolarizing current steps (*C*), and a 200-ms hyperpolarizing current step of −0.5 nA (*D*).

Table 2 summarizes the characteristics of the membrane properties of the DCN neurons from P25–26 rats. As can be seen in the table, DCN neurons from Paired, Unpaired, and Sit groups exhibited similar resting membrane potentials, threshold, current required for an evoked AP, AP amplitude, and AP duration. There was no significant difference in the number of evoked APs. For example, the number of evoked APs for the Paired group (16.73 ± 1.27), which was elicited at a 200-ms depolarizing current of 0.2 nA, is a bit higher than that for the Unpaired group (13.81 ± 1.61) and the Sit group (13.93 ± 2.03), but the difference was not statistically significant [$F(2, 51) = 1.202$, $P = 0.309$]. However, as shown in Fig. 4 *A* and *B* and confirmed by ANOVA, DCN neurons from Paired rats exhibited a significantly smaller after-hyperpolarization (AHP) amplitude [$F(2, 61) = 5.090$, $P < 0.01$] and shorter latency [$F(2, 61) = 3.177$, $P < 0.05$] for the first AP evoked by a 200-ms depolarizing current pulse, accompanied by a shorter interval between the first and second evoked APs (S1S2 interval). Post hoc comparisons revealed that the group effects in AHP amplitude were attributable to a significant difference between the Paired group and both the Unpaired and Sit groups ($P < 0.05$ and $P < 0.001$,

respectively). The group effects in latency were attributable to a significant difference between the Paired group and the Unpaired group ($P < 0.05$). The Paired group consistently exhibited shorter latency for evoked APs (21.79 ± 5.34 ms) than the Sit group (39.83 ± 7.70 ms), but the difference was not statistically significant ($P = 0.104$). Importantly, as shown in Fig. 4*C*, Pearson correlation analysis revealed a significant positive linear association between AHP amplitude and the percent of CRs on the fourth session in the Paired group ($R = 0.688$, $P < 0.05$) but not in the Unpaired group ($R = −0.06$, $P = 0.598$) or the Sit group ($R = −0.05$, $P = 0.869$). Moreover, although the mean level of responding was 40% CRs, responses ranged from 0 to 71.11% with well-conditioned rats generally showing smaller AHPs. Fig. 4*D* shows a waterfall plot of conditioned responses during EBC session 4 in a well-conditioned, freely moving rat and indicates well-timed responses against a relatively quiet baseline with occasional movements before the presentation of the tone CS. Therefore, our data suggest the changes in both AHP amplitude and latency in Paired rats are learning-related changes in intrinsic membrane properties in the cerebellum. This

Table 1. Comparison of membrane properties of evoked APs in fluorescent and nonfluorescent DCN neurons

PRV-152 fluorescent labeling	Vm, mV	Input resistance, MΩ	AP threshold, mV	Current required for evoked AP, nA	Latency, ms	Amplitude, mV	APD$_{50}$, ms	APD$_{50}$ rising, ms	APD$_{50}$ falling, ms	AHP, mV	S1S2 interval, ms
Unlabeled	−46.45 ± 0.46	103.75 ± 8.18	−46.85 ± 0.88	0.08 ± 0.01	31.72 ± 5.32	68.01 ± 1.71	0.80 ± 0.04	0.32 ± 0.01	0.48 ± 0.03	−10.50 ± 0.67	17.37 ± 2.16
Labeled	−45.64 ± 0.97	79.63 ± 6.87	−48.30 ± 1.13	0.10 ± 0.02	40.04 ± 8.52	68.25 ± 1.86	0.72 ± 0.07	0.29 ± 0.02	0.43 ± 0.04	−11.96 ± 1.19	29.99 ± 9.13

Note that there were no statistical differences in any measures for evoked APs between fluorescence-labeled ($n = 20$) and unlabeled ($n = 42$) DCN neurons. Vm, resting membrane potential.

www.manaraa.com

Table 2. Membrane properties of evoked DCN APs from conditioned P25–26 rats

Group	Vm, mV	Input resistance, MΩ	AP threshold, mV	Current required for evoked AP, nA	Latency, ms	Amplitude, mV	APD_{50}, ms	APD_{50} rising, ms	APD_{50} falling, ms	AHP, mV	S1S2 interval, ms
PD	−46.53 ± 0.74	104.26 ± 9.89	−48.16 ± 1.13	0.09 ± 0.02	21.79 ± 5.34*	66.63 ± 2.06	0.82 ± 0.05	0.33 ± 0.02	0.50 ± 0.03	−8.87 ± 0.81[†]	17.46 ± 3.33
UP	−45.52 ± 0.72	82.22 ± 8.86	−47.39 ± 1.23	0.08 ± 0.01	46.46 ± 10.22	69.82 ± 2.10	0.73 ± 0.07	0.30 ± 0.02	0.43 ± 0.05	−12.30 ± 1.06	25.41 ± 8.09
Sit	−46.54 ± 0.93	99.69 ± 13.82	−45.87 ± 1.35	0.08 ± 0.02	39.83 ± 7.70	68.29 ± 2.89	0.74 ± 0.07	0.30 ± 0.03	0.44 ± 0.05	−12.73 ± 1.17	21.65 ± 4.77

Cell numbers (n) for the Paired (PD), Unpaired (UP), and Sit groups were 26, 20, and 16 cells, respectively. Fluorescent cell numbers (n) for the PD, UP, and Sit groups were 8, 7, and 5 cells, respectively. Note that there were group differences in AHP amplitude and a marginal group difference in latency for evoked AP. The difference in AHP amplitude was between the PD group and the UP and Sit groups. The difference in latency was between the PD and UP group.
*$P = 0.055$.
[†]$P < 0.05$.

increased excitability may mediate the acquisition of conditioned eyeblink responses at this specific age.

Rebound Spikes. Table 3 summarizes the electrophysiological properties of rebound spikes (RD) for DCN neurons. As can be seen in Table 3, DCN neurons from the Paired, Unpaired, and Sit groups required similar currents for eliciting RD, and the amplitude and duration of RD were similar. There were no significant group dif-

ferences in the number of evoked RDs. For example, the number of evoked RDs for the Paired group (7.29 ± 1.15) elicited at a 200-ms hyperpolarizing current of −0.5 nA is a bit higher than that for the Unpaired group (6.40 ± 1.78) and the Sit group (5.67 ± 2.33), but the difference was not statistically significant [$F(2, 14) = 0.239$, $P = 0.791$]. There was also no significant group difference in the depth of hyperpolarization required to trigger RD [−159.79 ± 8.98 mV, 163.69 ± 8.62 mV, and 160.40 ± 6.60 mV, for the Paired, Unpaired,
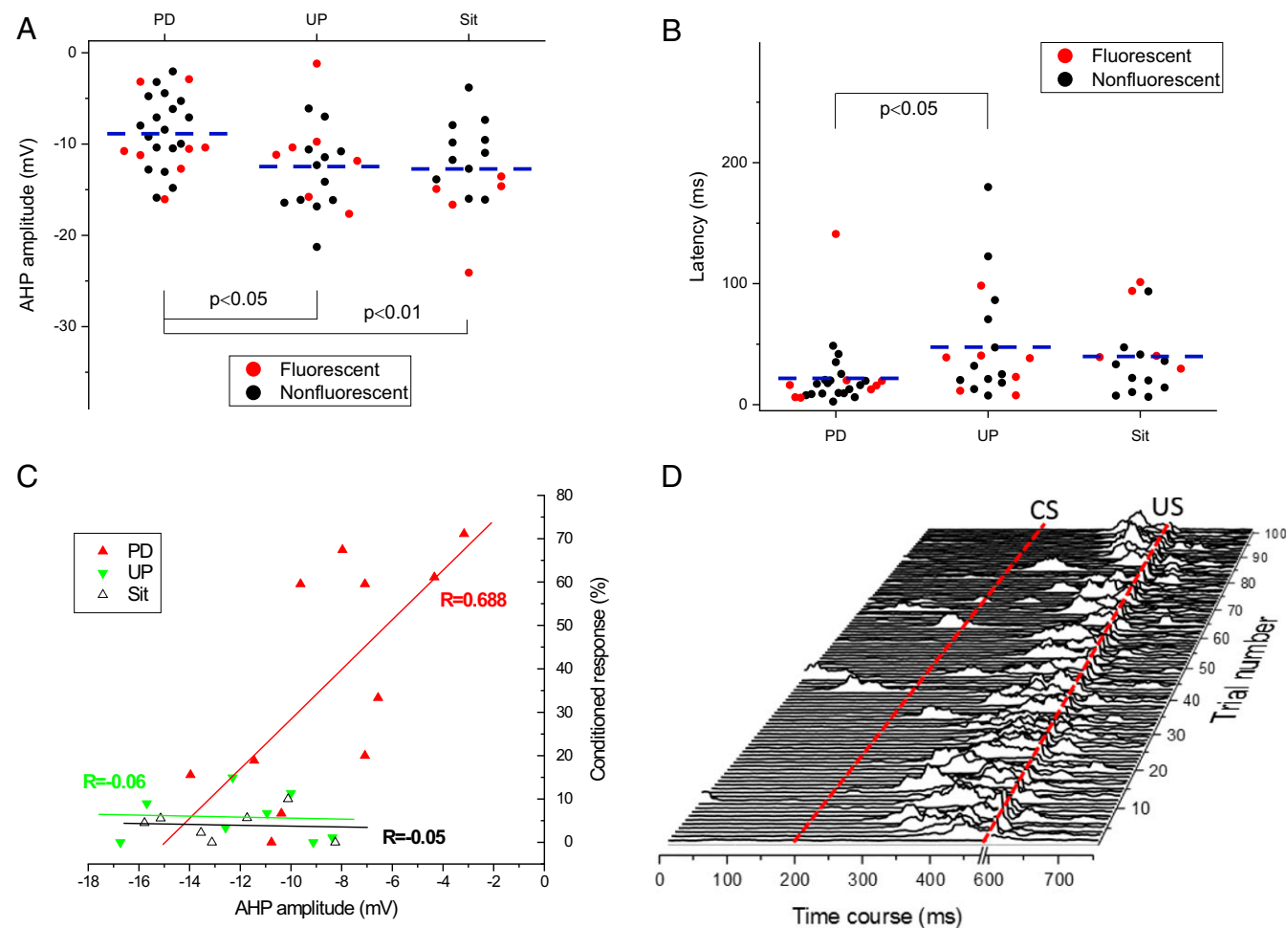

Fig. 4. Delay EBC produces learning-related changes in membrane properties of evoked DCN AP. (A–C) Learning-related changes in the evoked AP as a result of delay EBC were characterized by alterations in AHP amplitude (A), latency for evoked AP (B), and a positive linear association between AHP amplitude and percent CRs (CRs%) at the fourth session (C). Note that each point in the A and B represents the result from a single neuron (red solid circles for fluorescent neurons and black solid circles for nonfluorescent neurons), and the dashed line illustrates the average for each group. Each point in C represents the result from a single animal. (D) Representative eyelid EMG activity from a rat given paired conditioning during the last training session. Note that the rat had 71% CRs and a reduced AHP amplitude of −3.17 mV. Dashed lines indicate the onset times of the CS and US. A blanking circuit in operation during the US (the break in the x axis) prevented the shock from saturating the EMG amplifier.

Wang et al.

www.manaraa.com

Table 3. Summary of membrane properties of evoked DCN RDs from conditioned P25–26 rats

Group	RD threshold, mV	Current required for evoked RD, nA	Latency, ms	RD amplitude, mV	RD APD_{50}, ms	RD APD_{50} rising, ms	RD APD_{50} falling, ms	RD AHP, mV	RD S1S2, interval, ms
PD	$-54.50 \pm 1.20^*$	-0.71 ± 0.11	$48.89 \pm 12.78^*$	69.34 ± 2.40	0.85 ± 0.07	0.33 ± 0.02	0.52 ± 0.04	$-9.43 \pm 1.13^*$	14.08 ± 2.66
UP	-47.89 ± 1.18	-0.89 ± 0.16	111.97 ± 22.19	68.64 ± 2.21	0.76 ± 0.08	0.30 ± 0.03	0.46 ± 0.05	-13.25 ± 1.41	21.67 ± 5.21
Sit	-50.63 ± 1.87	-0.70 ± 0.14	101.57 ± 22.59	67.68 ± 3.25	0.82 ± 0.08	0.32 ± 0.03	0.50 ± 0.05	-11.87 ± 1.40	19.33 ± 2.84

Cell numbers (*n*) for the Paired (PD), Unpaired (UP), and Sit groups were 22, 14, and 15, respectively. Fluorescent cell numbers (*n*) for PD, UP, and Sit groups were 6, 6, and 4, respectively. Note that there were group differences in threshold, latency, and AHP amplitude. The difference in threshold and AHP amplitude was between the PD and UP group. The difference in latency was between the PD and UP and Sit groups.
*$P < 0.05$.

and Sit groups, respectively, $F(2, 49) = 0.055$, $P = 0.946$], which was induced by the hyperpolarization current steps when the cells were held at -70 mV baseline. However, Fig. 5 shows and an ANOVA confirmed that there were significant group differences in the RD threshold [$F(2, 49) = 5.886$, $P < 0.01$] and latency [$F(2, 49) = 3.830$, $P < 0.05$] for the first evoked RD spike elicited by a 200-ms hyperpolarizing current pulse, and there was a marginal difference in AHP amplitude [$F(2, 49) = 2.450$, $P = 0.09$]. Post hoc comparisons revealed the group effects in latency were attributable to a significant difference between the Paired group and both the Unpaired ($P <$

0.05) and the Sit ($P < 0.05$) group, and the group effects in threshold and AHP amplitude were attributable to a significant difference between the Paired group and the Unpaired group (all Ps < 0.05). Once again, as shown in Fig. 5*D*, correlation analysis revealed a positive linear relationship between the AHP amplitude of RDs and the percent of CRs on the fourth session in the Paired group ($R = 0.668$, $P < 0.05$) but not in either the Unpaired group ($R = -0.1$, $P = 0.830$) or the Sit group ($R = -0.34$, $P = 0.666$). These alterations in RDs that occurred in DCN neurons in P25–26 rats may contribute to the increased learning seen in the Paired rats at this specific age
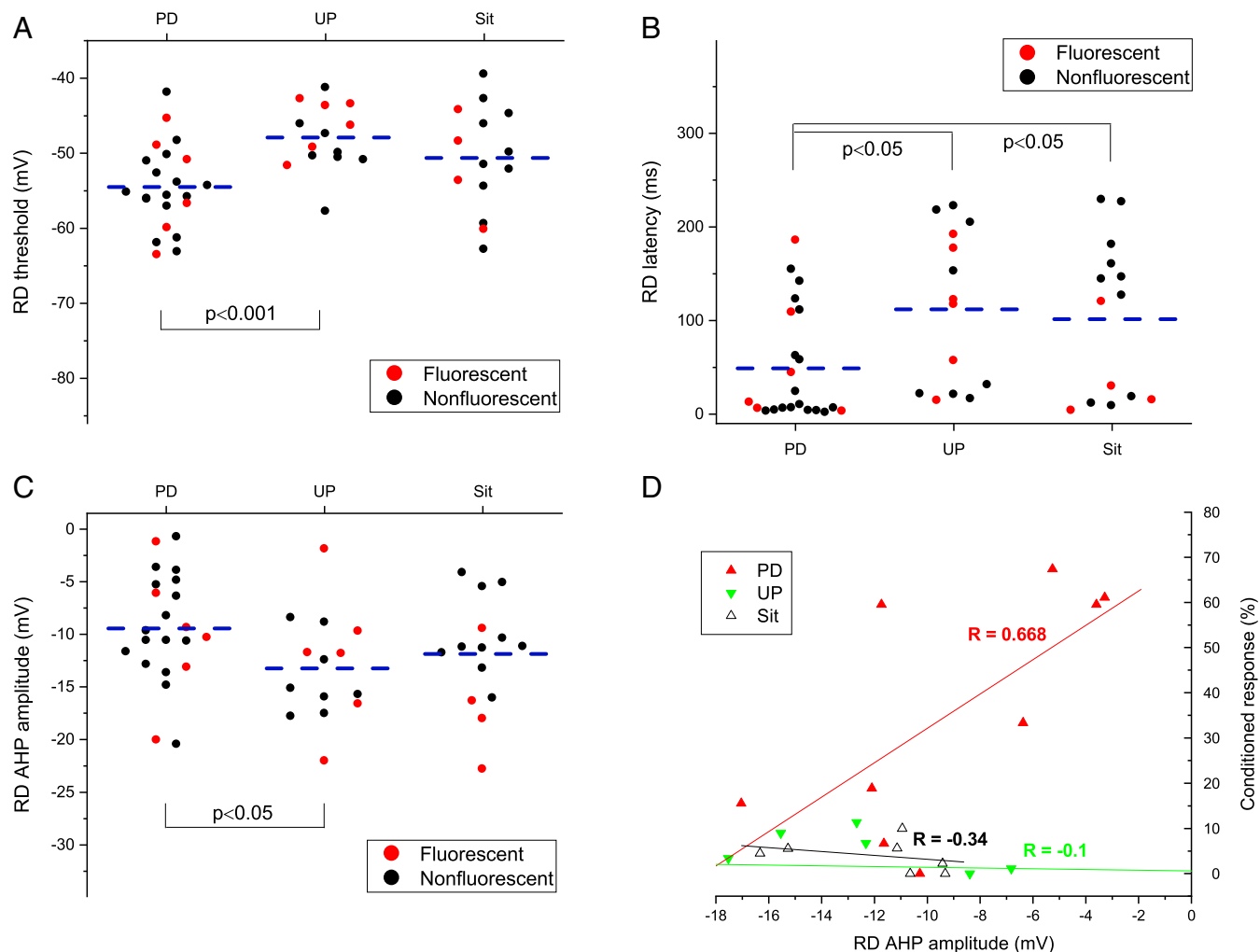

Fig. 5. Delay EBC produces learning-related changes in membrane properties of evoked DCN RDs. Note that learning-related changes as a result of delay EBC were characterized by alterations in RD threshold (*A*), latency for evoked RD (*B*), AHP amplitude (*C*), and a positive linear correlation between AHP amplitude and percent CRs (CRs%) at the fourth session (*D*). Each point in *A*–*C* represents the result from a single neuron (red solid circles for fluorescent neurons and black solid circles for nonfluorescent neurons), and the dashed lines illustrate the average for each group. Each point in *D* represents the result from a single animal.

Wang et al.

www.manaraa.com

because the DCN rebound phenomenon represents neural plasticity that was triggered by inhibitory inputs from cerebellar Purkinje cells, probably by the unique modes of cerebellar Purkinje cell activation induced by differential processing of the information from both the shock US climbing fiber and tone CS mossy fiber (35).

Discussion

In the present study we found that P25–26 rats with moderate levels of learning as a result of delay EBC compared with rats in the Unpaired and Sit groups showed significant changes in membrane properties of DCN neurons characterized by a reduced AHP amplitude and a shortened latency for an evoked AP. Similar findings were also observed for the hyperpolarization-elicited RDs. Most importantly, our data revealed a positive linear relationship between EBC and AHP amplitude for both evoked AP and RDs. Taken together, these changes in membrane properties represent an increased excitability of DCN neurons that may contribute to the acquisition of conditioned eyeblink responses at this specific age (14, 36).

The behavioral data showed that rats in the Paired group acquired a significantly greater percentage of conditioned eyeblink responses when trained with four sessions of delay tone–shock paired conditioning at P23–24 than rats in the Unpaired and Sit control groups. These findings are consistent with previous reports from Freeman and coworkers (4, 14, 36) showing the ontogeny of rat delay EBC may begin between P17 and P24 if using tone–shock pairings (4, 14, 36) and can develop as early as P12 if the immature auditory system is bypassed by direct stimulation of the pontine nuclei (17). Since we have recently developed a procedure for obtaining viable and healthy DCN slices from P25–26 rats for electrophysiological recordings (16), the moderate learning levels acquired at this specific age during delay EBC made it possible for us to map the learning-specific changes in membrane properties of DCN neurons even though a significant perineuronal net in DCNs had already developed (27).

Acquisition during delay EBC depends on the neural function of the cerebellum, including the cerebellar cortex and DCN. Neural function is determined by the intrinsic membrane properties and its responsiveness to synaptic inputs (37). Intrinsic plasticity and synaptic plasticity have been widely regarded as the cellular mechanisms underlying acquisition of learning and memory (3, 9, 38–42). Since both neuronal excitability and synaptic plasticity are mediated by intrinsic ion currents and share similar signal cascades (43, 44), alteration in ion currents could affect both neuronal excitability and synaptic plasticity. On the one hand, neuronal excitability could modulate the responsiveness of neurons to synaptic inputs. For example, transient increased neuronal excitability that occurs at the early phase of learning and memory could favor the facilitation of synaptic plasticity such as long-term potentiation (43); on the other hand, the changes in the balance of excitatory and inhibitory input could in turn modulate the level of depolarization and thus regulate neuronal intrinsic excitability (43, 45, 46). This positive feedback loop between neuronal excitability and synaptic plasticity contributes to learning and memory consolidation. Cerebellar learning could emerge because several forms of plasticity happen in succession. For example, widespread pairing-dependent increases in membrane excitability may set the stage for more input- and response-specific changes in the form of synaptic plasticity. Importantly, Disterhoft and coworkers (47–52) have noted that hippocampal conditioning-specific reductions in AHP are widespread (occurring throughout CA1 pyramidal neurons) but are transitory in nature, lasting several days before returning to baseline. On the other hand, Schreurs et al. (3) found that increases in Purkinje cell dendrite membrane excitability still existed a month after asymptotic levels of EBC. DCN neurons, a convergence site and the sole motor output pathway from cerebellum, may represent a functional convergence of both intrinsic excitability and synaptic integration to encode the signal in-

formation for cerebellar motor learning and memory (8, 53–55). Consistent with these previous reports, our DCN slice-recording data from P25–26 rats given delay EBC revealed a reduced AHP amplitude and shortened latency for evoked AP in rats that exhibited moderate levels of learning and a positive linear relationship between AHP amplitude and EBC. AHP has previously been reported to be important for regulating the spike frequency and accommodation in the hippocampus (38) and cerebellar cortex (3) and is widely regarded as an index of membrane excitability engaged in the process of learning and memory (3, 38, 39, 49, 50, 56–59). AHP increases can decrease the intrinsic excitability that has been correlated with cognitive decline in animals (60, 61), while AHP reduction can result in increased excitability that has been associated with the enhanced learning in conditioned animals versus controls (3, 38). Importantly, this conditioning-specific AHP reduction is independent of modification in synaptic properties (38). Therefore, the alteration in the membrane properties of DCN cells in Paired rats that received four sessions of delay EBC may be an early sign of learning-mediated changes, which may contribute to the robust acquisition others have observed at the sixth session of delay EBC at the same age (14, 36). These findings are in line with reports in awake behaving mice showing that facilitation in DCN may drive the eyelid movement and mediate the conditioned behavior (41, 42).

RD, which is another intrinsic property of DCN neurons and is modulated by synaptic inputs from Purkinje cells and climbing fibers (11, 54, 62, 63), is regarded as encoding the amplitude of inhibitory synapses in the cerebellar circuit, serving to transfer inhibitory signals, especially from Purkinje cells (64), and defining the accuracy and timing of cerebellar motor performance (13). Interestingly, a reduced AHP amplitude accompanied by alterations in the latency and RD threshold were also seen in RDs from P25–26 Paired rats, which suggests that synaptic inputs, especially the inhibitory inputs, may shape the neural state and its response to synaptic inputs and thus be involved in associative cerebellar learning (11, 13, 63). Taken together, our findings show that the membrane properties for evoked DCN RDs in Paired rats characterized by alterations in AHP latency and RD threshold represent another type of learning-related change that results from delay EBC. These results may help explain the increased acquisition of conditioned eyeblink responses at this specific age (15, 30, 36).

In this experiment we used PRV-152 as a transsynaptic neuronal tracer to identify DCN neurons responsible for the eyeblink response and found labeled third-order premotor neurons in DCN, including the dorsolateral anterior interpositus nucleus, after 3 d of PRV inoculation, similar to previous reports in rats (31), rabbits (28), and mice (32). The original purpose of injecting PRV-152 was to identify projection neurons controlling the eyeblink response to determine whether these third-order neurons comprised an "engram" for EBC (65). The fact that there were no consistent differences in electrophysiological measures between fluorescent and nonfluorescent neurons suggests that conditioning-specific changes in membrane excitability occurred in a large subset of neurons in the DCN in the same way that many pyramidal cells in the hippocampus and prefrontal cortex show conditioning-specific changes in membrane excitability (38, 39, 49, 56–58, 66, 67). The fact that PRV-152 is eventually lethal required us to determine a narrow window during which DCN neurons were healthy enough for recording regardless of whether they were fluorescent at the time of recording. Interestingly, we have found that without the constraint of recording viability, given sufficient time, many of the neurons in the DCN begin to fluoresce, as shown in Fig. 3, *Upper Inset*. This suggests that these cells were synaptically connected, because PRV-152 is transmitted only transsynaptically (68, 69). However, during the narrow recording window, there was more variability in the number of visibly labeled neurons, with very few fluorescent neurons in the DCN in some cases and many fluorescent cells in others.

Wang et al.

This variation may be explained by individual differences in the speed of retrograde labeling, in the site of inoculation, or in the angle of dissection and slice preparation. Of note is the number of cells that were fluorescent tended to increase in slices during incubation and within the recording session itself, demonstrating that viral replication continued in vitro. Finally, because our GFP reporter is tied to viral DNA, cells may not have been fluorescent even when they were infected if there was not enough viral DNA to express the fluorescent protein. These observations indicate that we cannot definitively determine that unlabeled cells were not part of the eyeblink pathway. Although it would have been ideal to record only from third-order cells that were fluorescent, because these would have been the cells most directly linked to the eyelid, the data taken together suggest that increased membrane excitability is a property of many cells in the DCN, a finding that is consistent with changes in excitability in other areas of the brain and that is a phenomenon that may require synaptic modifications to provide specificity (37).

Similar to previous reports from Enquist and coworkers (70, 71), fluorescent DCN cells exhibited a reduced input resistance compared with nonfluorescent cells, although the differences did not reach statistical significance. Previous studies (72, 73) have shown contradictory effects of PRV (also known as "herpes virus") infection on neuronal excitability. For example, there is a report of increased excitability of PRV-infected neurons in rat superior cervical ganglia at 32–38 h after PRV inoculation into the anterior chamber of the eye (72), but there is another report of reduced excitability in PRV-infected auditory brainstem neurons of Mongolian gerbils (73). In vitro and in vivo studies from Enquist and coworkers (70, 71, 74, 75) found that acute PRV infection could induce aberrant electrical activity and rapid firing, and the infection-induced firing was independent of synaptic input and may be related to electrical coupling induced by viral membrane fusion proteins. Importantly, this rapid firing was observed in PRV infection by virulent strains but not by attenuated strains such as PRV-152, a derivative of the Bartha strain of PRV, used here. These findings suggest the mechanisms underlying alterations in neuronal excitability induced by PRV infection may be complex and thus may not be simply the result of a general loss of membrane conductance or the disruption of transmembrane ion gradients (76). In the current study, PRV-152, an attenuated strain of PRV that has shown no dramatic alteration in the physiological properties of infected neurons (71, 74), was used as a transsynaptic tracer for the identification and characterization of DCN neurons involved in the eyeblink response, and those characteristics were no different from those in unlabeled DCN neurons in inoculated rats and in uninoculated rats. Future experiments may target DCN fluorescent neurons with optogenetic tools, including channelrhodopsins, and explore whether activation of these neurons is sufficient to evoke eyeblink response.

In summary, we demonstrate here that intrinsic membrane excitability in the DCN increased with EBC. These learning-specific changes in DCN excitability have not previously been reported in any species or task.

Materials and Methods

Subjects. P14 Long–Evans rats were supplied by Charles River Laboratories, housed in a cage with their littermates and mother, given free access to food and water, and maintained on a 12-h light/dark cycle. Rat pups were weaned and housed individually after P21. Rat pups were maintained in accordance with guidelines issued by the NIH, and the research was approved by the West Virginia University Animal Care and Use Committee.

Electromyography Electrode Implantation. At P21 rats were anesthetized with isoflurane (induction at 5% and maintained at 1–2%), and a headstage containing two wires for differential electromyography (EMG) recordings, one metal ground wire, and two twisted metal wires for bipolar periorbital shock administration (Plastics One Inc.) was implanted. Briefly, differential EMG electrodes were implanted in the left upper eyelid, a ground electrode was secured beneath the surface of skin, and bipolar shock-stimulating electrodes were implanted caudal to the left eye. After anesthesia induction, bupivacaine (<2 mg/kg) was injected at the incision site, and immediately following surgery, rats were given ketoprofen (5 mg/kg) and fluids (2 mL normal saline) s.c. Surgery was done 2 d before EBC so rats could recover from surgery.

PRV-152 Inoculation and Identification of DCN Putative Projection Neurons Involved in Eyeblink Control. PRV-152, a GFP-labeled retrograde transsynaptic tracer, was the kind gift of Lynn Enquist, Princeton University, Princeton. Procedures similar to those described in a previous publication (28) were used for PRV-152 inoculation and anti-PRV immunolabeling to identify PRV-labeled DCN neurons. Briefly, at P22–23, rats were anesthetized with 2% isoflurane, and 4 μL of PRV-152 at a concentration of 8.55×10^8 pfu/mL was injected into two sites in the orbicularis oculi muscle of the left upper eyelid. After PRV inoculation, when not undergoing EBC procedures, rats were maintained in a biosafety level 2 facility for 3.5 d to ensure that PRV was taken up by the axon terminals of facial nucleus neurons and then retrogradely transported to DCN projection neurons via the red nucleus (28) and that PRV-infected DCN neurons could be identified by fluorescence detection.

A separate set of five rats that did not undergo EMG implantation or EBC were used for anti-PRV immunolabeling to verify PRV labeling of the EBC motor output pathway. At 2.5, 3, and 3.5 d after PRV inoculation, rats were killed and transcardially perfused with PBS (pH 7.4) by a 4% formaldehyde fixative. Brains were removed and placed in fixative for storage and then were cryoprotected in 30% sucrose before being cut into 50-μm sections on a freezing microtome. First, free-floating sections were washed in 0.5 M Tris and were placed in 3% H_2O_2 for 30 min to block endogenous peroxidases. Second, sections were incubated in 10 mM citrate buffer (pH 3.0) at 37 °C for 30 min for antigen retrieval before being transferred to blocking solution (3% normal rabbit serum in 0.5 M Tris·Triton X-100) for 1 h. Third, sections were incubated with a goat anti-PRV primary antibody overnight at 4 °C and then were incubated with a secondary antibody (biotinylated rabbit anti-goat; 1:200) for 1 h. Finally, sections were put in VECTASTAIN ABC reagents (Vector Kit; Vector Laboratories) for 1 h followed by 3,3′-diaminobenzidine-tetrahydrochloride (Vector Kit; Vector Labs) for 2–5 min.

Rat EBC. The conditioning apparatus consisted of a sound-attenuating chamber (Colbourn) containing a Plexiglas cylinder and commutator (Plastics One, Inc.). The back wall of the sound-attenuating chamber had a small house light that stayed on during conditioning sessions, and a panel containing a speaker was mounted at a 45° angle above the cylinder. A light-weight cable connected to the headstage was attached to the commutator to allow free movement of the rat in the cylinder. From the commutator, a second cable was connected to an AC/DC differential amplifier (A-M Systems) and a stimulus isolator (365A; World Precisions Instruments). Computer software (LabVIEW 8.0; National Instruments) controlled stimulus delivery and recorded differential EMG activity that was filtered (300–3,000 Hz), amplified (5,000×), rectified, and integrated (20-ms time constant).

At P23, 29 rats of either sex from 10 litters were randomly assigned to one of three groups, Paired ($n = 13$, eight males and five females), Unpaired ($n = 9$, two males and seven females), or Sit ($n = 7$, two males and five females). The conditioning paradigm consisted of four training sessions across 2 d, with three sessions approximately 3 h apart on the first day and one session on the second day, each session with paired or explicitly unpaired presentations of a CS (a tone, 380 ms, 2.8 kHz, 88 dB) delivered through the speaker and a US (a periocular shock, 100 ms, 2–3.5 mA) delivered through a stimulus isolator. A blanking circuit in operation during the US prevented the shock from swamping the EMG signal.

Rats were given 5 min of habituation to the test chamber before each training session. Four training sessions were chosen not only because modest levels of learning could be seen by the fourth session of EBC (14, 36) but because, in pilot experiments, this was the point at which DCN projection neurons were first labeled with PRV, and there were no effects of PRV infection on the behavior or on the membrane properties of DCN neurons (see below).

Paired sessions consisted of 100 trials of delay EBC including 90 tone–shock paired trials and 10 tone-alone test trials occurring after every ninth paired trial to assess integrated EMG activity without the shock artifact. For paired trials, the interstimulus interval was 280 ms, and the stimuli coterminated. Trials were separated by an average intertrial interval (ITI) of 30 s, and sessions were separated by 3 h. Unpaired sessions consisted of 190 trials of explicitly unpaired presentations of the tone (100 trials, to equate with the total number of CS presentations during paired sessions) and shock (90 trials). The same stimulus durations were used as in the paired procedure. The ITI averaged 15 s to match the time spent in the conditioning chamber and the temporal distribution of stimuli in Paired groups. Rats in the Sit group

Wang et al.

www.manaraa.com

were placed in the training chamber without stimulus presentations for a duration equal to that of the rats in the Paired and Unpaired groups.

Conditioned responses were defined as EMG activity, starting 80 ms after CS onset to avoid the potential for alpha responses, that was eight SDs above the average baseline value during a 200-ms pre-CS period. If EMG activity 100 ms before CS onset was four SDs or more above baseline, the trial was omitted from analysis to ensure that movement or spontaneous blinking artifacts did not artificially inflate response levels.

Slice Preparation and Patch-Clamp Recordings. Procedures identical to those previously published (16, 77, 78) were used for slice preparation, electrophysiological recordings, and data analysis. Briefly, rats were rendered unconscious with carbon dioxide and then were decapitated. After brain removal, coronal cerebellar slices from the cerebellum were cut at 34 °C on a vibrating slicer (Leica VT1200S) with sucrose artificial cerebrospinal fluid (S-ACSF) containing (in mM) 200 sucrose, 2.5 KCl, 1.2 $MgCl_2$, 0.5 $CaCl_2$, 1.25 NaH_2PO_4, 26 $NaHCO_3$, and 20 dextrose. Slices were incubated for 1 h at 34 °C in 95% O_2-saturated and 5% CO_2-saturated ACSF containing (in mM) 125 NaCl, 3.0 KCl, 1.2 $MgSO_4$, 2.0 $CaCl_2$, 1.2 NaH_2PO_4, 26 $NaHCO_3$, and 10 dextrose and then were maintained at room temperature until electrophysiological recording. Vertical vibration of the blade was manually adjusted with a Vibrocheck device (Leica Biosystems) before slice preparation and was set to 0 μM.

A slice was placed in a modified recording chamber containing the bath solution (ACSF). DCN neurons were identified morphologically through a 40× water-immersion objective using differential interference contrast (DIC)-IR optics (Olympus BX50WI). PRV-infected neurons were identified by GFP under fluorescence optics. Whole-cell patch-clamp recordings were performed using an Axon MultiClamp 700B on cells with diameters of 15–20 μM in the interpositus and the medial portion of the lateral nucleus. These neurons are regarded as large glutamatergic projection neurons (26, 33). Generally, we made recordings in two to three cells of DCN slices from each rat. Patch pipettes made from borosilicate glass (1.5 mm o.d., 0.86 mm i.d.; catalog no. BF150-86-10; Sutter Instrument Company) were pulled with a P97 Brown–Flaming micropipette puller (Sutter Instrument Company). The final resistances of pipettes filled with the internal solution [containing

(in mM) 140 potassium gluconate ($C_6H_{11}O_7K$), 4.6 $MgCl_2\cdot6H_2O$, 10 Hepes, 10 EGTA, 4.0 Na_2ATP, pH 7.3 (KOH)] were between 5 and 8 MΩ. Data were low-pass filtered at 2 kHz and acquired at 20 kHz. Membrane properties were measured when the neuron had stabilized for 5 min after the whole-cell configuration was achieved. Quantitative analysis included resting membrane potential measured directly upon breakthrough in the whole-cell configuration, input resistance based on membrane potential changes due to depolarizing current injections immediately after whole-cell configuration, AP threshold (APH), current required for eliciting the first AP, the half-width of elicited AP (APD_{50}) including rising and falling phases, the amplitude of elicited AP, the number of elicited APs, latency to the first AP elicited by a 250-ms duration depolarizing current injection, peak amplitude of the AHP, S1S2 interval, the current required for hyperpolarization-induced RDs, and the properties of RDs. Recordings were accepted only if the resistance of the initial seal formations was greater than 1 GΩ and were rejected if their output was unstable or series resistance changed more than 20%. To obtain an accurate measurement of neuronal excitability independent of membrane potential changes, continuous direct current was applied through the recording electrode to hold the cell at a −70 mV baseline. All recordings were made at room temperature.

All electrophysiological data were recorded online using pCLAMP 10 software (Axon Instruments). Standard off-line analyses were conducted using Clampfit 10.0.

Data are presented as means ± SEM. One-way ANOVA followed by least significant difference post hoc comparisons was calculated in SPSS (Version 24; SPSS Inc.) with $P < 0.05$ as the criterion for significance.

1. Freeman JH, Jr, Nicholson DA (1999) Neuronal activity in the cerebellar interpositus and lateral pontine nuclei during inhibitory classical conditioning of the eyeblink response. *Brain Res* 833:225–233.
2. Gormezano I, Schneiderman N, Deaux E, Fuentes I (1962) Nictitating membrane: Classical conditioning and extinction in the albino rabbit. *Science* 138:33–34.
3. Schreurs BG, Gusev PA, Tomsic D, Alkon DL, Shi T (1998) Intracellular correlates of acquisition and long-term memory of classical conditioning in Purkinje cell dendrites in slices of rabbit cerebellar lobule HVI. *J Neurosci* 18:5498–5507.
4. Stanton ME, Freeman JH, Jr, Skelton RW (1992) Eyeblink conditioning in the developing rat. *Behav Neurosci* 106:657–665.
5. Christian KM, Thompson RF (2003) Neural substrates of eyeblink conditioning: Acquisition and retention. *Learn Mem* 10:427–455.
6. Nicholson DA, Freeman JH, Jr (2004) Selective developmental increase in the climbing fiber input to the cerebellar interpositus nucleus in rats. *Behav Neurosci* 118:1111–1116.
7. Steinmetz JE (2000) Brain substrates of classical eyeblink conditioning: A highly localized but also distributed system. *Behav Brain Res* 110:13–24.
8. Aizenman CD, Linden DJ (2000) Rapid, synaptically driven increases in the intrinsic excitability of cerebellar deep nuclear neurons. *Nat Neurosci* 3:109–111.
9. Pugh JR, Raman IM (2006) Potentiation of mossy fiber EPSCs in the cerebellar nuclei by NMDA receptor activation followed by postinhibitory rebound current. *Neuron* 51:113–123.
10. Pugh JR, Raman IM (2008) Mechanisms of potentiation of mossy fiber EPSCs in the cerebellar nuclei by coincident synaptic excitation and inhibition. *J Neurosci* 28:10549–10560.
11. Bengtsson F, Ekerot CF, Jörntell H (2011) In vivo analysis of inhibitory synaptic inputs and rebounds in deep cerebellar nuclear neurons. *PLoS One* 6:e18822.
12. Pugh JR, Raman IM (2005) GABAA receptor kinetics in the cerebellar nuclei: Evidence for detection of transmitter from distant release sites. *Biophys J* 88:1740–1754.
13. Witter L, Canto CB, Hoogland TM, de Gruijl JR, De Zeeuw CI (2013) Strength and timing of motor responses mediated by rebound firing in the cerebellar nuclei after Purkinje cell activation. *Front Neural Circuits* 7:133.
14. Freeman JH, Jr, Nicholson DA (2000) Developmental changes in eye-blink conditioning and neuronal activity in the cerebellar interpositus nucleus. *J Neurosci* 20:813–819.
15. Freeman JH, Jr, Nicholson DA (2004) Developmental changes in the neural mechanisms of eyeblink conditioning. *Behav Cogn Neurosci Rev* 3:3–13.
16. Wang D, Schreurs BG (2014) Maturation of membrane properties of neurons in the rat deep cerebellar nuclei. *Dev Neurobiol* 74:1268–1276.
17. Campolattaro MM, Freeman JH (2008) Eyeblink conditioning in 12-day-old rats using pontine stimulation as the conditioned stimulus. *Proc Natl Acad Sci USA* 105:8120–8123.
18. Goldsberry ME, Elkin ME, Freeman JH (2014) Sensory system development influences the ontogeny of eyeblink conditioning. *Dev Psychobiol* 56:1244–1251.
19. Freeman JH, Campolattaro MM (2008) Ontogenetic change in the auditory conditioned stimulus pathway for eyeblink conditioning. *Learn Mem* 15:823–828.
20. Horiuchi T, Kawahara S (2010) Effects of ipsilateral cerebellum ablation on acquisition and retention of classically conditioned eyeblink responses in rats. *Neurosci Lett* 472:148–152.
21. Freeman JH, Jr, Halverson HE, Poremba A (2005) Differential effects of cerebellar inactivation on eyeblink conditioned excitation and inhibition. *J Neurosci* 25:889–895.
22. Freeman JH, Jr, Rabinak CA, Campolattaro MM (2005) Pontine stimulation overcomes developmental limitations in the neural mechanisms of eyeblink conditioning. *Learn Mem* 12:255–259.
23. McCormick DA, Thompson RF (1984) Cerebellum: Essential involvement in the classically conditioned eyelid response. *Science* 223:296–299.
24. McCormick DA, Thompson RF (1984) Neuronal responses of the rabbit cerebellum during acquisition and performance of a classically conditioned nictitating membrane-eyelid response. *J Neurosci* 4:2811–2822.
25. Mueller AL, Davis A, Sovich S, Carlson SS, Robinson FR (2016) Distribution of N-acetylgalactosamine-positive perineuronal nets in the macaque brain: Anatomy and implications. *Neural Plast* 2016:6021428.
26. Huang S, Uusisaari MY (2013) Physiological temperature during brain slicing enhances the quality of acute slice preparations. *Front Cell Neurosci* 7:48.
27. Morales E, et al. (2004) Releasing the peri-neuronal net to patch-clamp neurons in adult CNS. *Pflugers Arch* 448:248–258.
28. Gonzalez-Joekes J, Schreurs BG (2012) Anatomical characterization of a rabbit cerebellar eyeblink premotor pathway using pseudorabies and identification of a local modulatory network in anterior interpositus. *J Neurosci* 32:12472–12487.
29. Ng KH, Freeman JH (2012) Developmental changes in medial auditory thalamic contributions to associative motor learning. *J Neurosci* 32:6841–6850.
30. Schreurs BG, Burhans LB, Smith-Bell CA, Mrowka SW, Wang D (2013) Ontogeny of trace eyeblink conditioning to shock-shock pairings in the rat pup. *Behav Neurosci* 127:114–120.
31. Morcuende S, Delgado-Garcia JM, Ugolini G (2002) Neuronal premotor networks involved in eyelid responses: Retrograde transneuronal tracing with rabies virus from the orbicularis oculi muscle in the rat. *J Neurosci* 22:8808–8818.
32. Sun LW (2012) Transsynaptic tracing of conditioned eyeblink circuits in the mouse cerebellum. *Neuroscience* 203:122–134.
33. Aizenman CD, Huang EJ, Linden DJ (2003) Morphological correlates of intrinsic electrical excitability in neurons of the deep cerebellar nuclei. *J Neurophysiol* 89:1738–1747.
34. de Zeeuw CI, Berrebi AS (1996) Individual Purkinje cell axons terminate on both inhibitory and excitatory neurons in the cerebellar and vestibular nuclei. *Ann N Y Acad Sci* 781:607–610.

Wang et al.

35. Hoebeek FE, Witter L, Ruigrok TJ, De Zeeuw CI (2010) Differential olivo-cerebellar cortical control of rebound activity in the cerebellar nuclei. *Proc Natl Acad Sci USA* 107:8410–8415.

36. Ivkovich D, Paczkowski CM, Stanton ME (2000) Ontogeny of delay versus trace eyeblink conditioning in the rat. *Dev Psychobiol* 36:148–160.

37. Lisman J, Cooper K, Sehgal M, Silva AJ (2018) Memory formation depends on both synapse-specific modifications of synaptic strength and cell-specific increases in excitability. *Nat Neurosci* 21:309–314.

38. Coulter DA, et al. (1989) Classical conditioning reduces amplitude and duration of calcium-dependent afterhyperpolarization in rabbit hippocampal pyramidal cells. *J Neurophysiol* 61:971–981.

39. Disterhoft JF, Coulter DA, Alkon DL (1986) Conditioning-specific membrane changes of rabbit hippocampal neurons measured in vitro. *Proc Natl Acad Sci USA* 83: 2733–2737.

40. Kim JJ, Thompson RF (1997) Cerebellar circuits and synaptic mechanisms involved in classical eyeblink conditioning. *Trends Neurosci* 20:177–181.

41. ten Brinke MM, et al. (2015) Evolving models of pavlovian conditioning: Cerebellar cortical dynamics in awake behaving mice. *Cell Rep* 13:1977–1988.

42. Ten Brinke MM, et al. (2017) Dynamic modulation of activity in cerebellar nuclei neurons during pavlovian eyeblink conditioning in mice. *eLife* 6:e28132.

43. Belmeguenai A, et al. (2010) Intrinsic plasticity complements long-term potentiation in parallel fiber input gain control in cerebellar Purkinje cells. *J Neurosci* 30: 13630–13643.

44. Shim HG, et al. (2017) Long-term depression of intrinsic excitability accompanied by synaptic depression in cerebellar Purkinje cells. *J Neurosci* 37:5659–5669.

45. D'Angelo E, De Zeeuw CI (2009) Timing and plasticity in the cerebellum: Focus on the granular layer. *Trends Neurosci* 32:30–40.

46. Sehgal M, Song C, Ehlers VL, Moyer JR, Jr (2013) Learning to learn–Intrinsic plasticity as a metaplasticity mechanism for memory formation. *Neurobiol Learn Mem* 105: 186–199.

47. Moyer JR, Jr, Power JM, Thompson LT, Disterhoft JF (2000) Increased excitability of aged rabbit CA1 neurons after trace eyeblink conditioning. *J Neurosci* 20:5476–5482.

48. Moyer JR, Jr, Thompson LT, Disterhoft JF (1996) Trace eyeblink conditioning increases CA1 excitability in a transient and learning-specific manner. *J Neurosci* 16:5536–5546.

49. Oh MM, Kuo AG, Wu WW, Sametsky EA, Disterhoft JF (2003) Watermaze learning enhances excitability of CA1 pyramidal neurons. *J Neurophysiol* 90:2171–2179.

50. Oh MM, Power JM, Thompson LT, Moriearty PL, Disterhoft JF (1999) Metrifonate increases neuronal excitability in CA1 pyramidal neurons from both young and aging rabbit hippocampus. *J Neurosci* 19:1814–1823.

51. Farmer GE, Thompson LT (2012) Learning-dependent plasticity of hippocampal CA1 pyramidal neuron postburst afterhyperpolarizations and increased excitability after inhibitory avoidance learning depend upon basolateral amygdala inputs. *Hippocampus* 22:1703–1719.

52. Zelcer I, et al. (2006) A cellular correlate of learning-induced metaplasticity in the hippocampus. *Cereb Cortex* 16:460–468.

53. Kleim JA, et al. (2002) Synapse formation is associated with memory storage in the cerebellum. *Proc Natl Acad Sci USA* 99:13228–13231.

54. Zheng N, Raman IM (2010) Synaptic inhibition, excitation, and plasticity in neurons of the cerebellar nuclei. *Cerebellum* 9:56–66.

55. Uusisaari M, Knöpfel T (2011) Functional classification of neurons in the mouse lateral cerebellar nuclei. *Cerebellum* 10:637–646.

56. de Jonge MC, Black J, Deyo RA, Disterhoft JF (1990) Learning-induced afterhyperpolarization reductions in hippocampus are specific for cell type and potassium conductance. *Exp Brain Res* 80:456–462.

57. Matthews EA, Linardakis JM, Disterhoft JF (2009) The fast and slow afterhyperpolarizations are differentially modulated in hippocampal neurons by aging and learning. *J Neurosci* 29:4750–4755.

58. McKay BM, Oh MM, Disterhoft JF (2013) Learning increases intrinsic excitability of hippocampal interneurons. *J Neurosci* 33:5499–5506.

59. Simkin D, et al. (2015) Aging-related hyperexcitability in CA3 pyramidal neurons is mediated by enhanced A-type K+ channel function and expression. *J Neurosci* 35: 13206–13218.

60. Kaczorowski CC, Disterhoft JF (2009) Memory deficits are associated with impaired ability to modulate neuronal excitability in middle-aged mice. *Learn Mem* 16: 362–366.

61. Landfield PW, Pitler TA (1984) Prolonged Ca2+-dependent afterhyperpolarizations in hippocampal neurons of aged rats. *Science* 226:1089–1092.

62. Aizenman CD, Linden DJ (1999) Regulation of the rebound depolarization and spontaneous firing patterns of deep nuclear neurons in slices of rat cerebellum. *J Neurophysiol* 82:1697–1709.

63. Person AL, Raman IM (2012) Synchrony and neural coding in cerebellar circuits. *Front Neural Circuits* 6:97.

64. Pedroarena CM (2010) Mechanisms supporting transfer of inhibitory signals into the spike output of spontaneously firing cerebellar nuclear neurons in vitro. *Cerebellum* 9:67–76.

65. Thompson RF (1976) The search for the engram. *Am Psychol* 31:209–227.

66. Santini E, Quirk GJ, Porter JT (2008) Fear conditioning and extinction differentially modify the intrinsic excitability of infralimbic neurons. *J Neurosci* 28:4028–4036.

67. Song C, Ehlers VL, Moyer JR, Jr (2015) Trace fear conditioning differentially modulates intrinsic excitability of medial prefrontal cortex-basolateral complex of amygdala projection neurons in infralimbic and prelimbic cortices. *J Neurosci* 35:13511–13524.

68. Banfield BW, Kaufman JD, Randall JA, Pickard GE (2003) Development of pseudorabies virus strains expressing red fluorescent proteins: New tools for multisynaptic labeling applications. *J Virol* 77:10106–10112.

69. Pickard GE, et al. (2002) Intravitreal injection of the attenuated pseudorabies virus PRV Bartha results in infection of the hamster suprachiasmatic nucleus only by retrograde transsynaptic transport via autonomic circuits. *J Neurosci* 22:2701–2710.

70. McCarthy KM, Tank DW, Enquist LW (2009) Pseudorabies virus infection alters neuronal activity and connectivity in vitro. *PLoS Pathog* 5:e1000640.

71. Smith BN, et al. (2000) Pseudorabies virus expressing enhanced green fluorescent protein: A tool for in vitro electrophysiological analysis of transsynaptically labeled neurons in identified central nervous system circuits. *Proc Natl Acad Sci USA* 97: 9264–9269.

72. Liao GS, Maillard M, Kiraly M (1991) Ion channels involved in the presynaptic hyperexcitability induced by herpes virus suis in rat superior cervical ganglion. *Neuroscience* 41:797–807.

73. Porres CP, Grothe B, Felmy F (2017) Breakdown of excitability by attenuated PRV-152 infection in auditory brainstem neurons of Mongolian gerbils. *Neuroscience* 367: 1–9.

74. Granstedt AE, Bosse JB, Thiberge SY, Enquist LW (2013) In vivo imaging of alphaherpesvirus infection reveals synchronized activity dependent on axonal sorting of viral proteins. *Proc Natl Acad Sci USA* 110:E3516–E3525.

75. Granstedt AE, Szpara ML, Kuhn B, Wang SS, Enquist LW (2009) Fluorescence-based monitoring of in vivo neural activity using a circuit-tracing pseudorabies virus. *PLoS One* 4:e6923.

76. Mayer ML, James MH, Russell RJ, Kelly JS, Pasternak CA (1986) Changes in excitability induced by herpes simplex viruses in rat dorsal root ganglion neurons. *J Neurosci* 6: 391–402.

77. Wang D, Schreurs BG (2010) Dietary cholesterol modulates the excitability of rabbit hippocampal CA1 pyramidal neurons. *Neurosci Lett* 479:327–331.

78. Wang D, Zheng W (2015) Dietary cholesterol concentration affects synaptic plasticity and dendrite spine morphology of rabbit hippocampal neurons. *Brain Res* 1622: 350–360.

79. Paxinos G, Watson C (2005) *The Rat Brain in Stereotaxic Coordinates* (Academic, Burlington, MA), 5th Ed.